Title	Stress State in the Kumano Basin and in Slope Sediment Determined From Anelastic Strain Recovery: Results From IODP Expedition 338 to the Nankai Trough
Author(s)	Oohashi, Kiyokazu; Lin, Weiren; Wu, Hung-Yu; Yamaguchi, Asuka; Yamamoto, Yuhji
Citation	Geochemistry, Geophysics, Geosystems (2017), 18(10): 3608-3616
Issue Date	2017-10
URL	http://hdl.handle.net/2433/254342
Right	An edited version of this paper was published by AGU. Copyright 2017 American Geophysical Union.
Type	Journal Article
Textversion	publisher

Stress State in the Kumano Basin and in Slope Sediment Determined From Anelastic Strain Recovery: Results From IODP Expedition 338 to the Nankai Trough

Kiyokazu Oohashi[1] [iD], Weiren Lin[2,3] [iD], Hung-Yu Wu[4] [iD], Asuka Yamaguchi[5] [iD], and Yuhji Yamamoto[6] [iD]

[1]Division of Earth Science, Biology, and Chemistry, Graduate School of Sciences and Technology for Innovation, Yamaguchi University, Yamaguchi, Japan, [2]Department of Urban Management, Graduate School of Engineering, Kyoto University, Kyoto, Japan, [3]Kochi Institute for Core Sample Research, Japan Agency for Marine-Earth Science and Technology, Nankoku, Japan, [4]Research and Development Center for Ocean Drilling Science, Japan Agency for Marine-Earth Science and Technology, Yokohama, Japan, [5]Department of Ocean Floor Geoscience, Atmosphere and Ocean Research Institute, The University of Tokyo, Chiba, Japan, [6]Center for Advanced Marine Core Research, Kochi University, Nankoku, Japan

Abstract Three-dimensional, in situ stresses in the Kumano Basin and slope sediment (IODP Sites C0002 and C0022) in the Nankai Trough, southwest Japan, have been determined using the anelastic strain recovery (ASR) of core samples. Two samples taken from Hole C0002J, located in the bottom of the Kumano Basin, indicate that the maximum principal stress, σ_1, is vertical. The intermediate principal stress, σ_2, is oriented ENE–WSW, parallel to the trench axis. These stress orientations are similar to those obtained using ASR and borehole breakout methods in previous expeditions. In contrast, a sample from the lower section of the slope sediment (Hole C0022B), located beneath the megasplay fault, is characterized by σ_1 plunging moderately to the ESE and σ_3 oriented near-horizontally, trending NNE–SSW. The direction of maximum horizontal stress obtained from ASR (WNW–ESE) is similar to that inferred from borehole breakouts in an adjacent hole (NW–SE). Trench-normal compression and a near-vertical σ_2 are also inferred from focal mechanisms of very-low-frequency earthquakes within the Nankai accretionary prism, and from borehole breakouts in the hanging wall of the megasplay fault. These observations suggest that the horizontal compressional regime extends to a shallower level than previously thought, likely due to the shallow portion of the megasplay fault accumulating tectonic stress in response to plate convergence.

1. Introduction

Stress-state analysis along active subduction zones is critical in understanding the accumulation and release of seismic energy throughout the earthquake cycle, and to constrain active tectonic processes (Lallemant & Funiciello, 2009). Determination of in situ stress is therefore a major objective of the NanTroSEIZE (Nankai Trough Seismogenic Zone Experiment) project. Borehole breakout analysis and hydraulic fracturing experiments were carried out in the accretionary prism and its cover sediments during the NanTroSEIZE project to determine horizontal stress orientations and magnitudes (e.g., Chang et al., 2010; Lin et al., 2010). The anelastic strain recovery (ASR) method is a straightforward way to determine three-dimensional in situ stress based on the time-dependent relaxation of recovered core samples (Lin et al., 2007; Matsuki, 1991). Borehole breakout and ASR analyses performed during NanTroSEIZE stages 1 and 2 indicate that the orientation of principal stresses in shallow sediments and the accretionary prism vary with distance from the trench (Figure 1a); i.e., NW–SE oriented maximum horizontal stress (S_{Hmax}) in the outer wedge to transition zone (e.g., IODP Sites C0004 and C0006: Chang et al., 2010), NE–SW oriented S_{Hmax} and σ_2 in the inner wedge (Site C0002: Byrne et al., 2009; Chang et al., 2010), and NW–SE trending S_{Hmax} in the center of the fore-arc basin (Site C0009: Lin et al., 2010). Sediments at the subduction input site (C0012) record a stress state with σ_1 oriented near vertically and show similar magnitudes of σ_2 and σ_3. It is therefore inferred that the sediments are in a "state of rest" (Yamamoto et al., 2013).

In 2012 and 2013, IODP (Integrated Ocean Drilling Program) Expedition 338 was carried out to deepen a preexisting hole that penetrates the Nankai accretionary prism as part of NanTroSEIZE stage 3 (Strasser
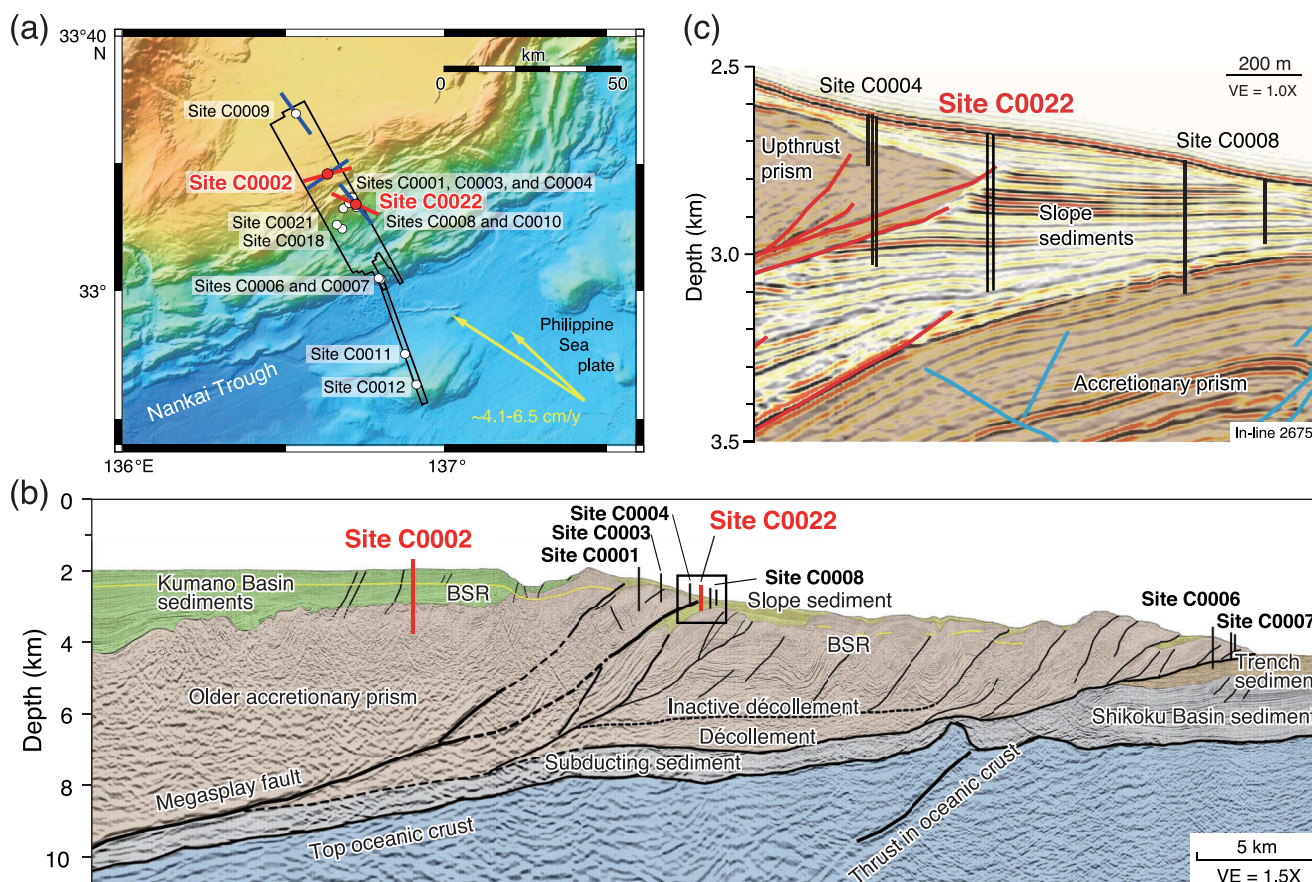
Figure 1. (a) Regional map showing the location of NanTroSEIZE drilling sites and in situ stress results from Sites C0002, C0022, and C0009. Red lines at drilling sites indicate the orientations of S_{Hmax} from ASR data obtained in this study. Blue lines show the orientations of S_{Hmax} estimated from borehole breakout data (C0002 from Chang et al., 2010 [data below 936 mbsf], C0022 from this study, and C0009 from Lin et al., 2010 [data below 1285 mbsf]). Boxed area indicates the region of the 3-D seismic survey. Arrows indicate the estimated convergence vectors between the Philippine Sea plate and the Japanese Islands (Heki, 2007; Seno et al., 1993). (b) Composite seismic profile extracted from 3-D seismic volume data (modified from Moore et al., 2009). Projected position of the NanTroSEIZE drilling sites is indicated. VE = vertical exaggeration. (c) Detailed seismic reflection profile in the vicinity of IODP Site C0022 (boxed area in Figure 1b). Red lines show branches of the megasplay fault and blue lines represent thrusts within the underlying accretionary prism (Kimura et al., 2011). Figures are modified from Strasser et al. (2014a, 2014c).

et al., 2014a). Here we present the results of ASR measurements conducted during Expedition 338 on core samples from the bottom of the Kumano Basin, and from slope sediment (Sites C0002 and C0022, respectively). We also present stress orientations (S_{Hmax}) obtained from borehole breakouts at Site C0022. We compare our results with stress orientations inferred from borehole breakouts as well as stress data obtained during the initial stages of NanTroSEIZE. Our results support previous ASR measurements at Site C0002 (Byrne et al., 2009) and provide the first report on the in situ stress state beneath the Nankai Trough megasplay fault at Site C0022.

2. Materials and Methods for ASR Measurements

Riserless drilling operations, including coring at the Kumano fore-arc basin Site C0002 and at slope basin Sites C0021 and C0022, were conducted during Expedition 338. During the operations, we acquired three high-quality intact core samples for ASR measurements, two at Site C0002 and one at Site C0022. Site C0002 is located at the southern edge of the Kumano Basin (Figure 1). Coring at Hole C0002J spanned 902–940 mbsf. Cores comprise calcareous silty claystone, interpreted as basal Kumano fore-arc basin sediment (lithologic Unit III), and noncalcareous silty claystone, interpreted as upper accretionary prism sediment (lithologic Unit IV); the boundary between lithologic Units III and IV was placed at 926.7 mbsf (Figure 2a) (Strasser et al., 2014b). We recovered two core samples for ASR analysis from depths of 903.4 and 922.9
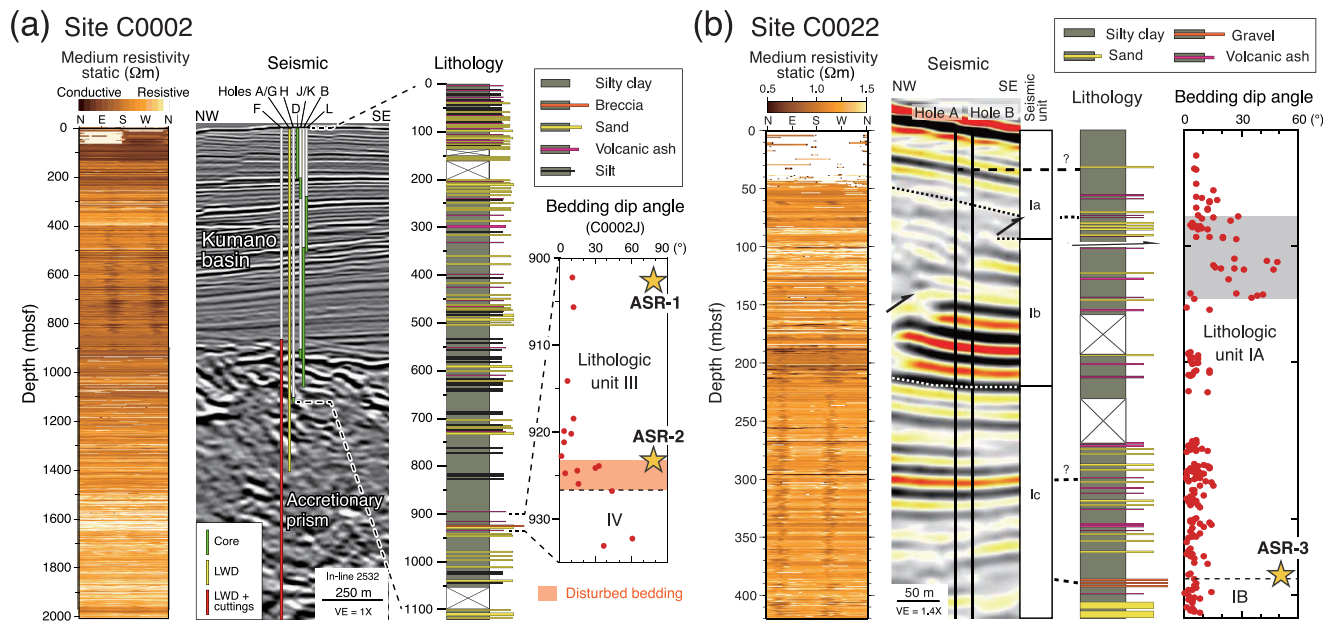
Figure 2. (a) Composite medium button resistivity image, seismic data, composite lithologic column for the core, and dip angle of bedding at (a) Site C0002 and (b) Site C0022. Locations of holes are projected onto the seismic line. Stars denote locations of ASR samples. Shaded section in Figure 2b shows interval with bedding dips of >20°. VE = vertical exaggeration.

mbsf (ASR-1 and ASR-2 from cores C0002J-1R-5 and C0002J-5R-5, respectively); hence, both samples are from basal sediment of the Kumano fore-arc basin (Figure 2a). Site C0022, located in the slope basin between previously drilled IODP Sites C0004 and C0008 (Expedition 314 Scientists, 2009a), was drilled through the uppermost 400 mbsf, close to the projected fault tip of the megasplay fault (Strasser et al., 2014c) (Figure 1c). Nearly continuous coring at Hole C0022B occurred from 0 to 420 mbsf (Figure 2b). The cores contain a slope basin succession dominated by silty clay (lithologic Subunit IA, 0–383.47 mbsf) and a lower slope basin interval characterized by mud-clast gravel (lithologic Subunit IB, 383.47–415.9 mbsf). Logging while drilling (LWD) resistivity images, and structural and porosity data from cores, as well as interstitial water data, suggest that the 80–140 mbsf interval is a plausible candidate for the location of the megasplay fault zone at Site C0022 (Strasser et al., 2014c). We acquired a sample for ASR analysis (ASR-3) from Core C0022B-38X-3, 50–71 cm at 384.7 mbsf (at ~245 m below the fault zone). All samples acquired for ASR analysis are coherent silty claystones without any bedding, visible disturbance or deformation structures under visual inspection and X-ray computed tomography (X-CT) imaging, hence, we regarded them as an isotropic material. The core samples were prepared for ASR analysis by following the procedures established by Lin et al. (2007) and applied by Byrne et al. (2009). After ASR measurement, paleomagnetic analyses were conducted to restore the directions of the principal stress axes to the geographic coordinates (for details, see Yamamoto et al., 2013). Errors of the paleomagnetic measurements (95% confidence angle) range ± 4.6°–5.3°.

3. Results

3.1. ASR Measurements

Anelastic strains recovered during the measurements ranged from 25 to 700 microstrains, which are sufficiently high relative to the internal accuracy of the measuring system, allowing the data to be used for three-dimensional stress analysis. Based on the measured anelastic normal strains, the anelastic strain tensor was calculated as a function of time (t) using a least squares analysis. The calculated results include the principal strain components $\varepsilon_{1,2,3}(t)$, the mean normal strain $\varepsilon_m(t)$, the ratio of the intermediate to the major principal strains, and the ratio of the minor to the major principal strains. Time-strain curves of the calculated three principal anelastic strains and the mean constant strain are shown in Figure 3. By assuming that the orientation of the principal anelastic strains was the same as the orientation of the principal in situ
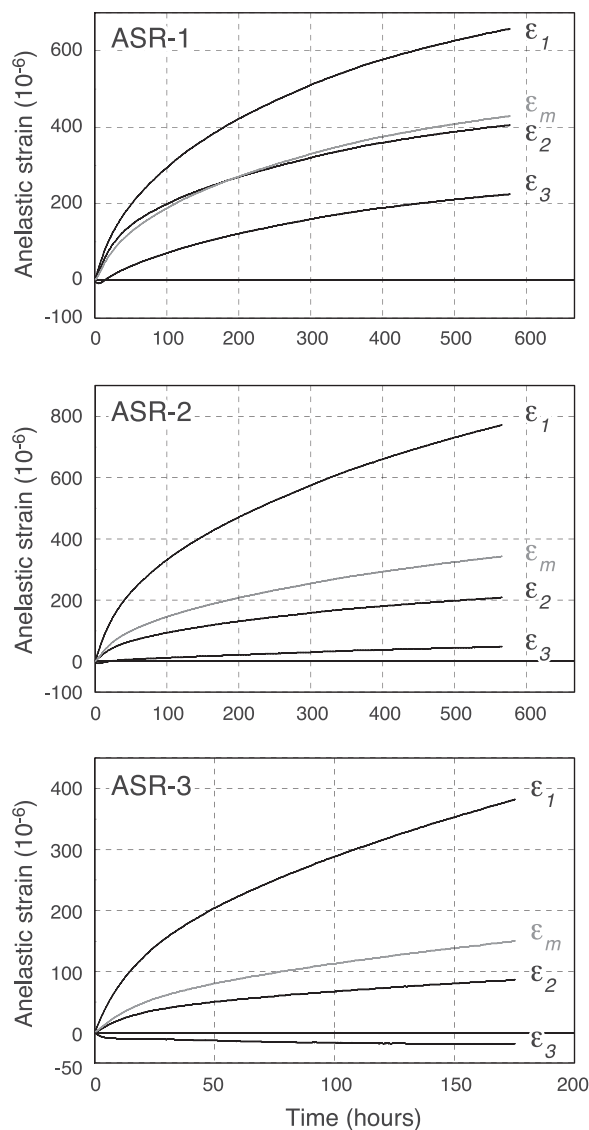
Figure 3. Three principal anelastic strains (ε_1, ε_2, ε_3) and mean strain (ε_m) versus time for each ASR sample.

stresses (Matsuki, 1991), we obtained three-dimensional in situ stress orientations (Figure 4) and ratios of principal stress deviations. We estimated the magnitudes of principal stresses by calculating the overburden stress (σ_v) and pore pressure (p_0) using the average density of the formations overlying the sample, and calculated the density of seawater under an assumption of hydrostatic pressure (for details, see Yamamoto et al., 2013).

The two samples from Hole C0002J yield nearly identical orientations of σ_1, σ_2, and σ_3 (where $\sigma_1 > \sigma_2 > \sigma_3$); the maximum principal stress (σ_1) is oriented vertically, and the intermediate principal stress (σ_2) is oriented ENE–WSW, parallel to the trench axis (Figure 4). S_{Hmax} and the minimum horizontal stress (S_{hmin}) are oriented ENE–WSW (072°–075°) and NNW–SSE (162°–165°), respectively. The stress magnitudes of samples from 903.4 and 922.9 mbsf are $\sigma_1 = \sim$37–38 MPa, $\sigma_2 = \sim$32–35 MPa, and $\sigma_3 = \sim$30–34 MPa. The sample from Hole C0022B displays plunging axes of principal stresses, with σ_1 plunging moderately (35°) toward the ESE and σ_3 plunging gently (18°) toward the SSW (Figure 4). S_{Hmax} and S_{hmin} are oriented WNW–ESE ($\sim$114°) and NNE–SSW ($\sim$024°), respectively. The stress magnitudes are $\sigma_1 = \sim$37–38 MPa, $\sigma_2 = \sim$33 MPa, and $\sigma_3 = \sim$31–32 MPa.

3.2. Borehole Breakouts

During drilling, concentrated stress caused by pore pressure, mud weight, and horizontal principal stresses occurs around the borehole wall. The azimuth of the maximum compressive stress around the wall is parallel to the direction of horizontal minimum principal stress (Zoback, 2007). Rock failures occur in pairs, 180° apart if the compressive stress is greater than the strength of the rock, a process known as borehole breakout. Observations of borehole breakout in LWD images provide a method to determine stress orientations during scientific drilling (Lin et al., 2010; Wu et al., 2013). At Site C0002, LWD was conducted only for Hole C0002F during Expedition 338. Hole C0002F shows only few breakouts in LWD images (Strasser et al., 2014b) due to the use of riser drilling. Hence, we infer the stress orientation in Hole C0002F from results of a previous expedition (S_{Hmax} of 41° ± 14° at Hole C0002A; Chang et al., 2010) because we observed no major fault/fracture between the two holes. In contrast, vertical and paired compressive failures, indicating stress-induced borehole breakout, are clearly observed in the borehole wall of Hole C0022A (Figure 2b). The breakout results indicate a consistent direction of S_{hmin} throughout the hole (Figure 5a). Breakout widths are between 30° and 90°. Because a borehole will generally remain stable during riserless drilling when wellbore breakout failure width is less than 90°, resistivity images of Hole C0022A were collected in a well-controlled borehole. Borehole breakouts were obtained from 50 mbsf and maintain a consistent orientation down to 400 mbsf (Figure 5a), passing through the megasplay fault. The preferred orientation of the breakouts (51° ± 8°; Figure 5b) implies that S_{Hmax} trends 141° ± 8°, which is approximately consistent with the plate convergence vector (Heki, 2007; Seno et al., 1993) (see Figure 1a). Comparison with observations from Hole C0002A indicates a $\sim$90° rotation of S_{Hmax} and a dramatic change in stress field between the slope basin and fore-arc basin sites. Breakout widths displayed in Figure 5b show the interaction between the local stress field and the borehole wall. The average breakout width in Hole C0022A is 37° ± 15°.

4. Discussion

4.1. Stress State at the Seaward Edge of the Kumano Basin (Site C0002)

ASR results from the two samples recovered from the bottom of the Kumano Basin at Hole C0002J indicate a vertical σ_1, a NNW–SSE-oriented σ_3, and S_{Hmax} oriented ENE–WSW. These stress orientations are comparable, but rotated $\sim$20° clockwise (viewed down), with those obtained previously from Hole C0002B (subvertical σ_1 axis; σ_3 axis trending NW–SE; Byrne et al., 2009). This difference of angle between the two measurements is within a combined error of the ASR method ($<$20°; Nagano et al., 2015) and
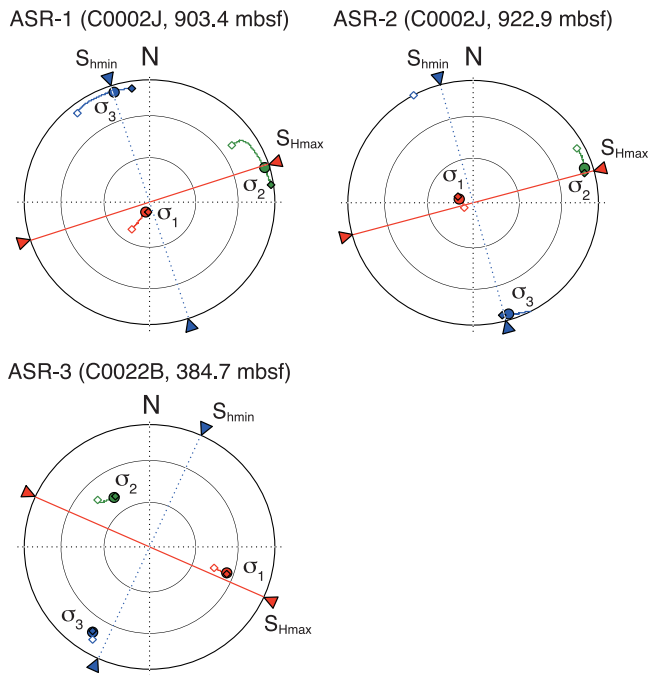
ASR-1 (C0002J, 903.4 mbsf)   ASR-2 (C0002J, 922.9 mbsf)

ASR-3 (C0022B, 384.7 mbsf)

Figure 4. Lower hemisphere, equal area projections of principal stress orientations determined by ASR analyses. S_{Hmax} and S_{hmin} are calculated based on the ASR results. Open and filled diamonds for each stress axis show the orientation at the start and end of the ASR measurement, respectively. Mean orientations of the stress axes are shown in the circle.

paleomagnetic measurement ($\sim5°$). Hole C0002J is located about 60 m northeast of Hole C0002B. The wellheads of the holes are situated at similar depths, and cores were recovered from 884.3 and 911.8 mbsf (Byrne et al., 2009) and 903.4 and 922.9 mbsf for this study. Bedding near the ASR core samples is subhorizontal to gently dipping ($<15°$) at Holes C0002B and C0002J (Expedition 315 Scientists, 2009; Strasser et al., 2014b). In addition, there are no differences in sedimentary facies between the cores used in the previous and present studies. The 3-D seismic reflection data from Site C0002 (Moore et al., 2009) also indicate bedding dipping to the northwest at $<15°$ at the interval where the ASR core samples were obtained. The depth of the lithologic boundary between Units III and IV was constrained to ~922 and 926.7 mbsf for Holes C0002B and C0002J, respectively. We can therefore assume that Holes C0002B and C0002J are lithologically and structurally continuous, and that there are no pre-existing anisotropies that could affect the stress state. In addition, the direction of S_{Hmax} inferred from borehole breakouts at Hole C0002A ($41° \pm 14°$; Chang et al., 2010), located ~80 m west of Hole C0002B, is consistent with our ASR results. Hence, the three-dimensional stress orientations obtained by ASR measurements can be considered a regional background stress state for the base of the Kumano Basin at Site C0002, which was stable between 2007 (Expedition 315) and 2012 (Expedition 338).

4.2. Stress State of the Slope Basin (Site C0022)
ASR results from the slope sediments at Hole C0022B indicate subhorizontal compression with σ_1 trending WNW–ESE, apparently parallel to the plate convergence vector. Borehole breakouts in the interval from ~50 to 420 mbsf (within the hanging wall and footwall of the projected megasplay fault) at Hole C0022A indicate that S_{Hmax} is oriented NW–SE, consistent with that calculated from ASR results (see Figure 1a). Core-scale minor faults in Hole C0022B are clustered in two intervals: 50–83 mbsf in the hanging wall and 386–405 mbsf in the footwall. The latter faults are located immediately below where we acquired the sample for ASR measurement (384.7 mbsf). In the hanging wall of the megasplay fault, minor faults are generally steeply dipping and preferentially strike NW–SE, whereas faults in the footwall show two preferred strikes of NW–SE and NE–SW, and shallow dips. This difference in fault orientation suggests the sediments were subjected to different stress conditions in the hanging wall and footwall of the megasplay fault (Strasser et al., 2014c). However, kinematic constraints for faults in the hanging wall and footwall, determined on split core surfaces and X-CT images, consistently indicate normal sense of shear. In addition, the faults are generally healed, lack cataclastic deformation, and are associated with clay smears along their surfaces, indicating early stage soft-sediment deformation. These observations suggest the core-scale faults formed under a range of different stress states, likely when the sediments were at a much shallower depth in the slope basin.

4.3. Across-Trench Variations in Stress State Near the Megasplay Fault
In the initial stages of NanTroSEIZE, the stress state around the megasplay fault was analyzed at Sites C0001, C0004, C0010, and C0006. Here we briefly summarize this stress state, and then discuss across-trench variations in stress near the tip of the megasplay fault. At Site C0001, located ~3 km landward from the seafloor trace of the megasplay fault (Figure 1b), analysis of borehole breakouts and drilling-induced tensile fractures provided the orientation, ratios, and magnitudes of the principal stresses for the hanging wall of the megasplay fault (Expedition 314 Scientists, 2009a). S_{Hmax} is consistently oriented NNW–SSE ($\sim335°$) throughout the measured interval from 80 to ~950 mbsf. At shallow depths (<500 mbsf), S_{Hmax} is interpreted to be σ_2 and smaller in magnitude than the vertical stress, indicating a normal faulting regime (Chang et al., 2010; Song et al., 2011). In contrast, S_{Hmax} at deeper depths (>500 mbsf) is interpreted to be σ_1, likely due to increasing S_{Hmax}, reflecting a change with depth from a normal faulting to a strike-slip regime (Chang et al., 2010). Borehole breakouts at Site C0004, located ~300 m landward from Site C0022, penetrated the megasplay fault at ~350 mbsf (Figure 1c) and consistently indicate S_{Hmax} oriented NW–SE throughout the measured interval of 80–400 mbsf (Expedition 314 Scientists, 2009b). Yamada and
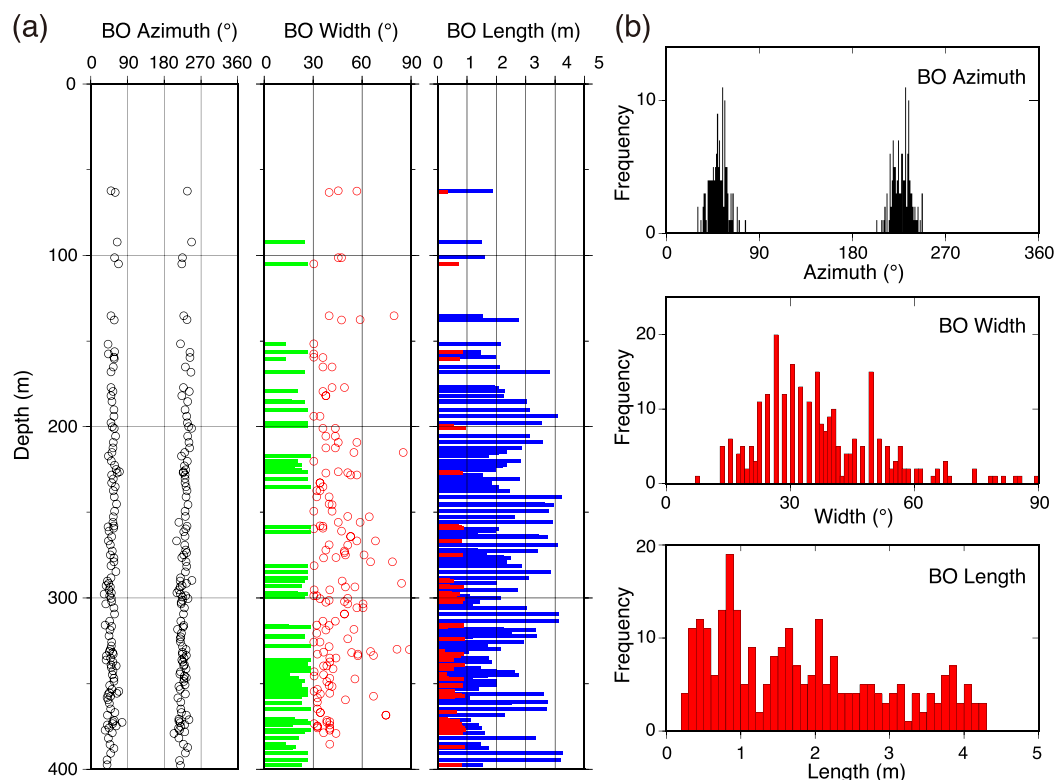
Figure 5. (a) Orientations (azimuth), widths, and lengths of borehole breakouts (BO) plotted against depth in Hole C0022A. Breakout widths less than 30° and breakout lengths shorter than 1 m are displayed as green and red bars, respectively. (b) Histograms of the orientations, widths, and lengths of borehole breakouts in Hole C0022A.

Shibanuma (2015) suggested that S$_{Hmax}$ at this site represents σ_1, based on stress magnitude estimations. In contrast, the borehole breakouts at Site C0010, located ~3 km southwest along the trench from Site C0004, show a downhole change in the orientation of the breakouts across the megasplay fault (about 20°–30° counterclockwise, looking down) (Expedition 319 Scientists, 2010), and McNeill et al. (2010) proposed that the megasplay fault represents a sharp mechanical discontinuity. Alternatively, Olcott and Saffer (2012) suggested that stress is not completely decoupled across the megasplay fault because σ_1 remains horizontal throughout the borehole, although they recognized a distinct shift to lower stress magnitudes over a 150 m section below the megasplay fault. At ~20 km seaward from Site C0022, Site C0006 penetrated the hanging wall and footwall of the frontal thrust (Expedition 314 Scientists, 2009c). Borehole breakouts over the measured interval, from 200 to ~700 mbsf, show that S$_{Hmax}$ is oriented NW–SE (150° ± 16°), consistent with results from Sites C0001 and C0004. ASR results by Byrne et al. (2009) from the hanging wall of the frontal thrust show a steeply plunging σ_1 with σ_3 trending northeast, indicating normal faulting and trench-parallel extension, similar to the shallow depths at Site C0001.

These data, combined with results from Site C0022, suggest a change in stress regime from normal faulting and trench-parallel extension at the frontal prism, to strike slip or thrusting with apparently trench-normal compression at both the hanging wall and footwall of the megasplay fault, to normal faulting and trench-normal extension at the seaward edge of the Kumano Basin. Lin et al. (2015) suggest a change in stress state from a normal faulting regime at shallow levels to a strike-slip or thrusting regime at deeper levels at all sites from NanTroSEIZE Stages 1 and 2, except for a NW–SE trending subhorizontal σ_1 observed immediately above the megasplay fault (Sites C0004 and C0010). Our results from Site C0022, from immediately beneath the megasplay fault, suggest a strike-slip or thrusting regime at shallow depths. A stress field with trench-normal compression and vertical σ_2 is also estimated from very-low-frequency (VLF) earthquakes that occur at 4–8 km depth in the Nankai accretionary prism off the Kii Peninsula (Ito et al., 2009). Trench-normal compression at shallow depths in the slope sediments supports the hypothesis that the horizontal compression regime extends to a much shallower level (i.e., into slope sediments) in the accretionary prism than previously

proposed (see Lin et al., 2015, Figure 3). This may occur due to the shallow portion of the megasplay fault accumulating tectonic stress in response to plate convergence. On the other hand, strike-slip or thrust faulting stress regimes were not recognized in the hanging wall of the frontal thrust (Byrne et al., 2009). We therefore speculate that, in contrast to the megasplay fault, the hanging wall of the décollement is not strongly coupled to the subducting footwall (e.g., Lewis et al., 2013) at shallow structural levels, possibly due to the weakness of the décollement (Byrne and Fisher, 1990). The coupling of the hanging wall and footwall of the shallow portion of the megasplay fault may play an important role in rupture propagation from the deep seismogenic zone to the seafloor. Conceptionally, if the coupling strength is high enough, and the fault does not show slip-weakening behavior, propagating rupture from the depths may be interrupted at there (like a "stuck in the mud" scenario indicated by Faulkner et al., 2011). In contrary, when the fault shows slip-weakening behavior in response to the high-velocity frictional sliding, large coseismic slip at the shallow portion of the megasplay fault, and resultant tsunami generation are expected to occur (e.g., Oohashi et al., 2015; Ujiie et al., 2013).

S_{Hmax} for Hole C0022B obtained from the ASR method is not normal to the ENE–WSW trending trench axis (20°–45° anticlockwise, looking down) but parallel to the plate convergence vector between the Philippine Sea plate and SW Japan (see Figure 1a). Since this deviation of angle is larger than the error of the ASR method, the difference is considered to be significant. Although in situ stress data of the frontal prism are not sufficient for a detailed discussion of the spatial distribution of stress, one explanation can be made for this oblique S_{Hmax}, as explained below. The model of strain partitioning along an oblique subduction margin states that the strike-slip component of relative plate motion is partitioned behind the fore arc as a trench-parallel strike-slip fault system, especially for the margins dominated by trench-parallel component (e.g., the Sumatran fault system in the Sumatra subduction zone, Fitch, 1972; McCaffrey, 2009). However, Martin et al. (2010) and Tsuji et al. (2014) observed strike-slip faults between the inner and outer wedges of the Nankai Trough and proposed that these faults in the accretionary prism play a key role in accommodating strike-slip motion resulting from oblique subduction of the Philippine Sea plate. In such a setting, trench-normal S_{Hmax} in the outer wedge is expected to rotate anticlockwise toward the trench-parallel direction with approaching transition zone between the inner and outer wedges (see Tsuji et al., 2014, Figure 8). Hence we infer that dextral strike-slip motion in the transition zone is responsible for the anticlockwise rotation of S_{Hmax} observed at Hole C0022B.

5. Conclusions

Three-dimensional, in situ stresses in the Kumano Basin and slope sediment in the Nankai Trough region of southwest Japan have been determined using ASR of core samples. The main results of this study are summarized as follows.

1. Two samples taken from the bottom of the Kumano Basin (Hole C0002J, depths of 903.4 and 922.9 mbsf) record a vertical σ_1, and σ_2 oriented ENE–WSW, parallel to the trench axis. These stress orientations are consistent with those obtained previously using the ASR method and borehole breakouts at the same site. This consistency between two independent measurements during IODP Expeditions 315 and 338 confirms the stability of the stress state, and the technical reliability of the ASR method.
2. The sample from immediately beneath the megasplay fault (Hole C0022B, 384.7 mbsf) shows that σ_1 plunges moderately to the ESE, and σ_3 is subhorizontal and trends NNE–SSW. The orientation of S_{Hmax} obtained from ASR measurements (WNW–ESE) is consistent with the direction interpreted from borehole breakout analysis (NW–SE).
3. The subhorizontal compression and steep σ_2 observed in the footwall of the megasplay fault indicate a strike-slip or thrusting stress regime rather than normal faulting even at shallow depths. This result indicates that the horizontal compression regime extends to a much shallower level of the accretionary prism, possibly due to the shallow portion of the megasplay fault accumulating tectonic stress in response to plate convergence. Rotation of S_{Hmax} within the outer wedge may suggest strain partitioning of the strike-slip component of oblique subduction in the transition zone between the inner and outer wedges.

References

Byrne, T., & Fisher, D. (1990). Evidence for a weak and overpressured décollement beneath sediment-dominated accretionary prisms. *Journal of Geophysical Research: Solid Earth*, *95*(B6), 9081–9097. https://doi.org/10.1029/JB095iB06p09081

Byrne, T. B., Lin, W., Tsutsumi, A., Yamamoto, Y., Lewis, J. C., Kanagawa, K., . . . Kimura, G. (2009). Anelastic strain recovery reveals extension across SW Japan subduction zone. *Geophysical Research Letters*, 36, L23310. https://doi.org/10.1029/2009GL040749

Chang, C., McNeill, L. C., Moore, J. C., Lin, W., Conin, M., & Yamada, Y. (2010). In situ stress state in the Nankai accretionary wedge estimated from borehole wall failures. *Geochemistry, Geophysics, Geosystems*, 11, Q0AD04. https://doi.org/10.1029/2010GC003261

Expedition 314 Scientists. (2009a). Expedition 314 Site C0001. In M. Kinoshita et al. (Eds.), *Proceedings of the Integrated Ocean Drilling Program* (Vols. 314/315/316). Washington, DC: Integrated Ocean Drilling Program Management International. https://doi.org/10.2204/iodp.proc.314315316.113.2009

Expedition 314 Scientists. (2009b). Expedition 314 Site C0004. In M. Kinoshita et al. (Eds.), *Proceedings of the Integrated Ocean Drilling Program* (Vols. 314/315/316). Washington, DC: Integrated Ocean Drilling Program Management International. https://doi.org/10.2204/iodp.proc.314315316.116.2009

Expedition 314 Scientists. (2009c). Expedition 314 Site C0006. In M. Kinoshita et al. (Eds.), *Proceedings of the Integrated Ocean Drilling Program* (Vols. 314/315/316). Washington, DC: Integrated Ocean Drilling Program Management International. https://doi.org/10.2204/iodp.proc.314315316.118.2009

Expedition 315 Scientists. (2009). Expedition 315 Site C0002. In M. Kinoshita et al. (Eds.), *Proceedings of the Integrated Ocean Drilling Program* (Vols. 314/315/316). Washington, DC: Integrated Ocean Drilling Program Management International. https://doi.org/10.2204/iodp.proc.314315316.124.2009

Expedition 319 Scientists. (2010). Site C0010. In D. Saffer (Ed.), *Proceedings of the Integrated Ocean Drilling Program* (Vol. 319). Tokyo, Japan: Integrated Ocean Drilling Program Management International. https://doi.org/10.2204/iodp.proc.319.104.2010

Faulkner, D. R., Mitchell, T. M., Behnsen, J., Hirose, T., & Shimamoto, T. (2011). Stuck in the mud? Earthquake nucleation and propagation through accretionary forearcs. *Geophysical Research Letters*, 38, L18303. https://doi.org/10.1029/2011GL048552

Fitch, T. J. (1972). Plate convergence, transcurrent faults, and internal deformation adjacent to Southeast Asia and the western Pacific. *Journal of Geophysical Research*, 77(23), 4432–4460. https://doi.org/10.1029/JB077i023p04432

Heki, K. (2007). Secular, transient, and seasonal crustal movements in Japan from a dense GPS array: Implication for plate dynamics in convergent boundaries. In T. H. Dixon & J.C. Moore (Eds.), *The seismogenic zone of subduction thrust faults* (pp. 512–539). New York, NY: Columbia University Press.

Ito, Y., Asano, Y., & Obara, K. (2009). Very-low-frequency earthquakes indicate a transpressional stress regime in the Nankai accretionary prism. *Geophysical Research Letters*, 36, L20309. https://doi.org/10.1029/2009GL039332

Kimura, G., Moore, G., Strasser, M., Screaton, E., Curewitz, D., Streiff, C., & Tobin, H. (2011). Spatial and temporal evolution of the megasplay fault in the Nankai Trough. *Geochemistry, Geophysics, Geosystems*, 12, Q0A008. https://doi.org/10.1029/2010GC003335

Lallemant, S., & Funiciello, F. (2009). *Subduction zone geodynamics*. Berlin, Germany: Springer. https://doi.org/10.1007/978-3-540-87974-9

Lewis, J. C., Byrne, T. B., & Kanagawa, K. (2013). Evidence for mechanical decoupling of the upper plate at the Nankai subduction zone: Constraints from core-scale faults at NanTroSEIZE Sites C0001 and C0002. *Geochemistry, Geophysics, Geosystems*, 14, 620–633. https://doi.org/10.1029/2012GC004406

Lin, W., Byrne, T. B., Kinoshita, M., McNeill, L. C., Chang, C., Lewis, J. C., . . . Kanamatsu, T. (2015). Distribution of stress state in the Nankai subduction zone, southwest Japan and a comparison with Japan Trench. *Tectonophysics*, 692, 120–130. https://doi.org/10.1016/j.tecto.2015.05.008

Lin, W., Doan, M.-L., Moore, J. C., McNeill, L., Byrne, T. B., Ito, T., . . . Kido, Y. (2010). Present-day principal horizontal stress orientations in the Kumano forearc basin of the southwest Japan subduction zone determined from IODP NanTroSEIZE drilling Site C0009. *Geophysical Research Letters*, 37, L13303. https://doi.org/10.1029/2010GL043158

Lin, W., Yeh, E.-C., Ito, H., Hirono, T., Soh, W., Wang, C.-Y., . . . Song, S.-R. (2007). Preliminary results of stress measurement using drill cores of TCDP Hole-A: An application of anelastic strain recovery method to three dimensional in situ stress determination. *Terrestrial, Atmospheric and Oceanic Sciences*, 18, 379–393. https://doi.org/10.3319/TAO.2007.18.2.379(TCDP)

Martin, K. M., Gulick, S. P. S., Bangs, N. L. B., Moore, G. F., Ashi, J., Park, J.-O., . . . Taira, A. (2010). Possible strain partitioning structure between the Kumano fore-arc basin and the slope of the Nankai Trough accretionary prism. *Geochemistry, Geophysics, Geosystems*, 11, Q0AD02. https://doi.org/10.1029/2009GC002668

Matsuki, K. (1991). Three-dimensional in-situ stress measurement with anelastic strain recovery of a rock core. In W. Wittke (Ed.), *Proceedings of the 7th International Congress on Rock Mechanics* (pp. 557–560). Aachen, Germany: International Society for Rock Mechanics.

McCaffrey, R. (2009). The tectonic framework of the Sumatran subduction zone. *Annual Review of Earth and Planetary Sciences*, 37, 345–366. https://doi.org/10.1146/annurev.earth.031208.100212

McNeill, L. C., Saffer, D. M., Byrne, T., Araki, E., Toczko, S., Eguchi, N., . . . Expedition 319 Scientists. (2010). IODP Expedition 319, NanTroSEIZE stage 2: First IODP riser drilling operations and observatory installation towards understanding subduction zone seismogenesis. *Scientific Drilling*, 10, 4–13. https://doi.org/10.2204/iodp.sd.10.01.2010

Moore, G. F., Park, J.-O., Bangs, N. L., Gulick, S. P., Tobin, H. J., Nakamura, Y., . . . Taira, A. (2009). Structural and seismic stratigraphic framework of the NanTroSEIZE Stage 1 transect. In M. Kinoshita et al. (Eds.), *Proceedings of the Integrated Ocean Drilling Program* (Vols. 314/315/316). Washington, DC: Integrated Ocean Drilling Program Management International. https://doi.org/10.2204/iodp.proc.314315316.102.2009

Nagano, Y., Lin, W., & Yamamoto, K. (2015). In-situ stress analysis using the anelastic strain recovery (ASR) method at the first offshore gas production test site in the eastern Nankai Trough, Japan. *Marine and Petroleum Geology*, 66, 418–424. https://doi.org/10.1016/j.marpetgeo.2015.02.027

Olcott, K. A., & Saffer, D. M. (2012). *Constraints on in situ stress across the shallow megasplay fault offshore the Kii Peninsula, SW Japan from borehole breakouts*. Paper presented at 2012 Fall Meeting, American Geophysical Union, San Francisco, CA.

Oohashi, K., Hirose, T., Takahashi, M., & Tanikawa, W. (2015). Dynamic weakening of smectite-bearing faults at intermediate velocities: Implications for subduction zone earthquakes. *Journal of Geophysical Research: Solid Earth*, 120, 1572–1586. https://doi.org/10.1002/2015JB011881

Seno, T., Stein, S., & Gripp, A. E. (1993). A model for the motion of the Philippine Sea plate consistent with Nuvel-1 and geological data. *Journal of Geophysical Research*, 98(B10), 17941–17948. https://doi.org/10.1029/93JB00782

Song, I., Saffer, D. M., & Flemings, P. B. (2011). Mechanical characterization of slope sediments: Constraints on in situ stress and pore pressure near the tip of the megasplay fault in the Nankai accretionary complex. *Geochemistry, Geophysics, Geosystems*, 12, Q0AD17. https://doi.org/10.1029/2011GC003556

Strasser, M., Dugan, B., Kanagawa, K., Moore, G. F., Toczko, S., Maeda, L., . . . Yamaguchi, A. (2014a). Expedition 338 summary. In M. Strasser et al. (Eds.), *Proceedings of the Integrated Ocean Drilling Program* (Vol. 338). Yokohama, Japan: Integrated Ocean Drilling Program. https://doi.org/10.2204/iodp.proc.338.101.2014

Strasser, M., Dugan, B., Kanagawa, K., Moore, G. F., Toczko, S., Maeda, L., . . . Yamaguchi, A. (2014b). Site C0002. In M. Strasser et al. (Eds.), *Proceedings of the Integrated Ocean Drilling Program* (Vol. 338). Yokohama, Japan: Integrated Ocean Drilling Program. https://doi.org/10.2204/iodp.proc.338.103.2014

Strasser, M., Dugan, B., Kanagawa, K., Moore, G. F., Toczko, S., Maeda, L., . . . Yamaguchi, A. (2014c). Site C0022. In M. Strasser et al. (Eds.), *Proceedings of the Integrated Ocean Drilling Program* (Vol. 338). Yokohama, Japan: Integrated Ocean Drilling Program. https://doi.org/10.2204/iodp.proc.338.107.2014

Tsuji, T., Ashi, J. & Ikeda, Y. (2014). Strike-slip motion of a mega-splay fault system in the Nankai oblique subduction zone. *Earth, Planets and Space*, *66*, 120. https://doi.org/10.1186/1880-5981-66-120

Ujiie, K., Tanaka, H., Saito, T., Tsutsumi, A., Mori, J. J., Kameda, J., . . . 343T Scientists. (2013). Low coseismic shear stress on the Tohoku-oki megathrust determined from laboratory experiments. *Science*, *342*, 1211–1214. https://doi.org/10.1126/science.1243485

Wu, H.-Y., Chan, C.-H., Kinoshita, M., & Saito, S. (2013). Stress field observation and modeling from the NanTroSEIZE scientific drillings in the Nankai Trough system, SW Japan. *Tectonophysics*, *600*, 99–107. https://doi.org/10.1016/j.tecto.2013.04.009

Yamada, Y., & Shibanuma, J. (2015). Small-scale stress fluctuations in borehole breakouts and their implication in identifying potential active faults around the seismogenic megasplay fault, Nankai Trough, SW Japan. *Earth Planets Space*, *67*, 17. https://doi.org/10.1186/s40623-014-0176-9

Yamamoto, Y., Lin, W., Oda, H., Byrne, T., & Yamamoto, Y. (2013). Stress states at the subduction input site, Nankai subduction zone, using anelastic strain recovery (ASR) data in the basement basalt and overlying sediments. *Tectonophysics*, *600*, 91–98. https://doi.org/10.1016/j.tecto.2013.01.028

Zoback, M. D. (2007). *Reservoir geomechanics*. Cambridge, UK: Cambridge University Press.